香港天文台
HONG KONG OBSERVATORY

Reprint 443

Radar-based Analyses on the Hailstorm of 9 April 2001

E.S.T. Lai & P.W. Li

Proceedings of International Conference
on Mesoscale Meteorology and Typhoon in East Asia,
Taipei, 26-28 September 2001

RADAR-BASED ANALYSES ON THE HAILSTORM OF 9 APRIL 2001

Edwin S.T. Lai and P. W. Li
Hong Kong Observatory, Hong Kong

1. INTRODUCTION

In the sub-tropical clime of Hong Kong, thunderstorms can occur throughout the summer months. Hailstorms, in contrast, are not that common, averaging only once every year and mostly confined to the high-risk months of March and April during the transition of seasons from winter to summer. Reports of earlier hailstorm cases in Hong Kong were mainly through the perspective of radar observations (Lam, 1981 and Lee et al. 1996). With the introduction of more observational platforms in recent years, it would be interesting to see how other data types augment or enrich the radar-based analyses.

Traditionally, forecasting the onset of heavy rain relies on synoptic pattern recognition and instability analyses. Increasing reliability in NWP guidance in recent years have rendered the task that much easier. Nevertheless, enhanced convection embedded within the mesoscale convective complex remains too elusive to predict. Depending on subtle changes on the finer spatial and temporal scales, towering cumulus may, or may not, develop into supercells or get organized into multicell systems, that eventually give rise to hailstones or violent squalls. This study explores how the problem may be tackled on a nowcasting basis, with emphasis on frequently updated local scale analysis and real-time radar monitoring.

Background information on the hailstorm event of 9 April 2001 is summarized in Section 2. Section 3 shows how various systems operated by the Hong Kong Observatory within the local observational network, in particular the automatic weather stations (AWS) and Doppler radar, work together to keep track of the hailstorm development. Section 4 attempts to assemble a conceptual hailstorm configuration from the various pieces of observational information so as to explore the likely hailstorm signatures in Doppler patterns. Finally, discussion and thoughts on future directions in hailstorm nowcasting are given in Section 5.

Edwin S.T. Lai, Hong Kong Observatory,
134A Nathan Road, Kowloon, Hong Kong.
Email: stlai@hko.gov.hk

2. BACKGROUND

Under the influence of a warm and humid maritime airstream, conditions on 9 April were generally cloudy and foggy to start with. Convergence effect was enhanced later in the day as a cooler easterly airstream advanced down the coast of southeastern China. Thunderstorms developed explosively to the northwest of Hong Kong over the Pearl River estuary. The skies grew ominously dark as day was turned into night in the late afternoon. Bands of squally thunderstorms swept across the territory in quick succession, bringing more than 50 millimetres of rain in three hours between 3 p.m. (07 UTC) and 6 p.m. (10 UTC). The last batch of storms to pass through Hong Kong was especially intense. Between 5:35 p.m. and 5:50 p.m., hailstones of up to 2.5 cm in diameter battered the city centre and the Victoria Harbour as the storm moved out to the open seas on a southeastward track (Fig. 1).

Synoptically, southern China was under an upper westerly regime with cyclonic southwesterlies and signs of weak troughing at the lower levels. Near the surface, the building-up of a ridge along the coast of southeastern China brought the easterlies to the doorstep of the Pearl River. With a moisture-laden lower troposphere already in generally unstable conditions (K-index higher than 30), enhanced convergence and daytime surface heating over the inland region triggered off intense convection west of the estuary. Severe thunderstorms so formed were swept along by the upper westerlies towards Hong Kong. A layer of very dry air in the mid-troposphere capping a moist lower layer in the pre-storm ascent at 00 UTC on 9 April was a classic set-up favouring the development of severe convection. The vertical profiles from the Observatory's ORSM (Operational Regional Spectral Model) analyses before and after the hailstorm showed a significant moistening of the mid-troposphere (Fig. 2). Although the surface precipitation predicted was never as intense as actual, ORSM did correctly forecast the mid-level moistening in its 00 UTC run (Fig. 3), showing the process to be convection-driven and the effect confined to a localized pocket near the Pearl River estuary.

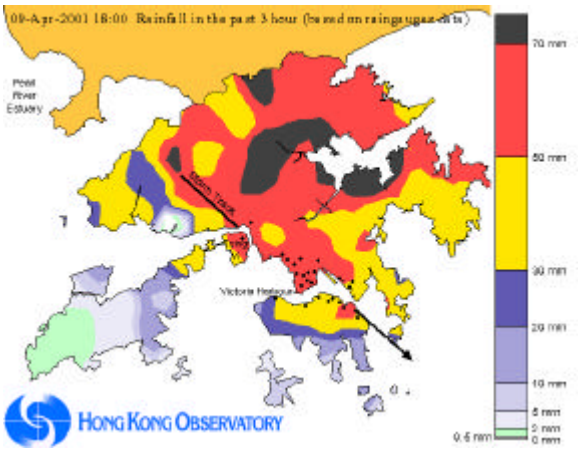

Fig. 1 - Rainfall (mm) distribution between 3 p.m. and 6 p.m. on 9 April 2001, with heavy dots showing the trail of hailstone reports spreading southeastwards across Hong Kong between 5:35 p.m. and 5:50 p.m. that day.

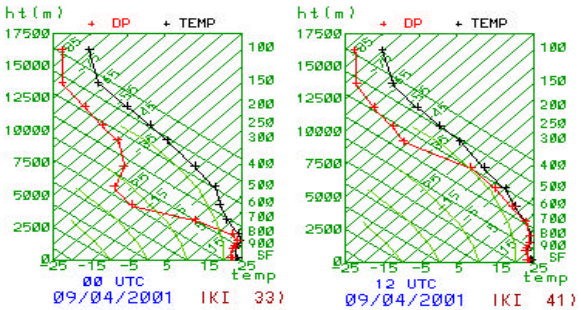

Fig. 2 - Tephigrams from ORSM analyses at 00 UTC (left) and 12 UTC (right) on 9 April 2001, showing a significant moistening of the mid-troposphere after the passage of the hailstorm.

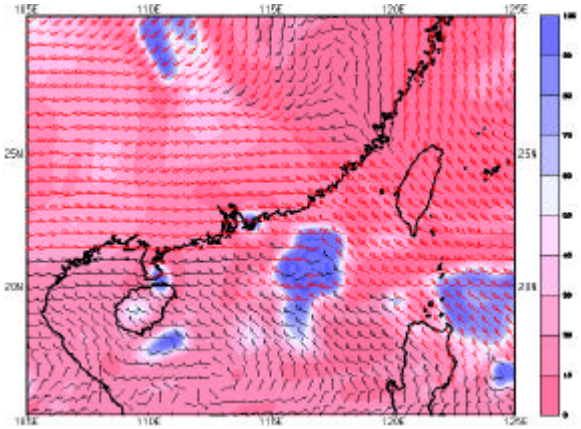

Fig. 3 - ORSM 8-hour forecast of 500-hPa wind and relative humidity fields, valid at 4 p.m. on 9 April 2001. A moist pocket was forecast to develop right over Hong Kong. In reality, the extent of moistening in the mid-troposphere was even more widespread and persistent.

3. OBSERVATIONAL EVIDENCES

3.1 Surface convergence and divergence lines

Local prevailing winds were easterly ahead of the hailstorm. At the Observatory, winds turned northwesterly and picked up after 5:30 p.m. In the next 15 minutes, temperatures rose slightly and relative humidity dropped. As hails began to fall at the Observatory, temperatures fell by about 1 °C, relative humidity rose and winds increased to about 15 m s^{-1}. After the passage of the hailstorm, winds settled back to an easterly direction and temperatures gently recovered. The whole event took no more than 20 minutes. Given that the speed of storm movement (from northwest to southeast) as estimated from radar was about 60 km hr^{-1}, the storm dimension was of the order of 20 km across, consistent with the vertical section derived from radar reflectivity.

Surface streamline analyses based on AWS winds showed a distinct convergence line running about 10 km ahead of a divergence line. The divergence line could be interpreted as the downdraft, creating a gust front that collided with the prevailing easterlies along the convergence line. With the storm system tracking southeastwards, the convergence line moved into the northwestern part of Hong Kong soon after 5 p.m. By 5:30 p.m. when hailstones started to be reported near Tsing Yi area (Fig. 1), the convergence line was right on top of the radar at Tate's Cairn with the divergence line following through another 10 km to the northwest (Fig. 4).

Fig. 4 - AWS winds at 5:30 p.m., with the pair of convergence (solid) and divergence (dashed) lines as implied from the streamline analysis.

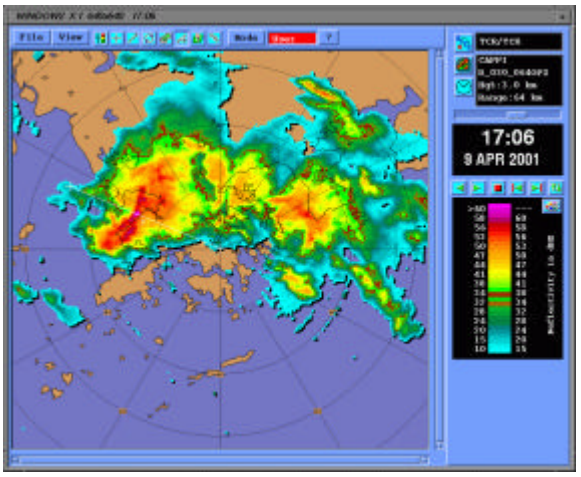

(a) 3-km CAPPI reflectivity at 5:06 p.m.

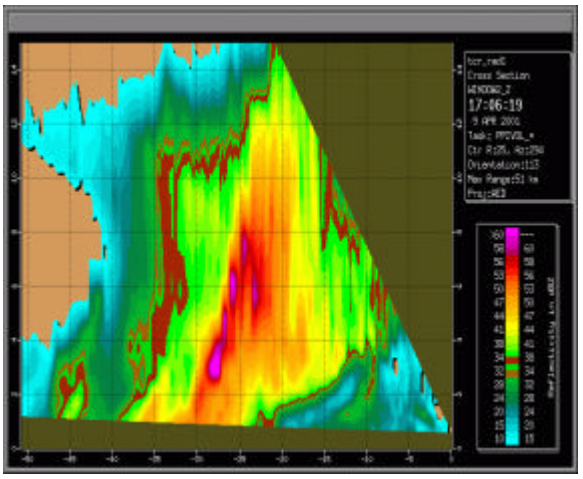

(b) Vertical section along X - Y for (a)

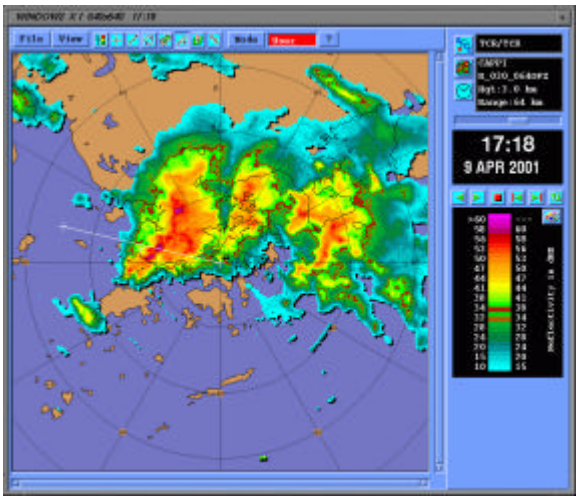

(c) 3-km CAPPI reflectivity at 5:18 p.m.

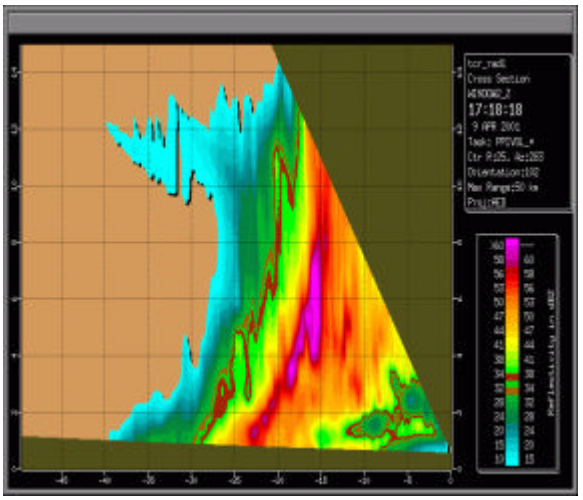

(d) Vertical section along X - Y for (c)

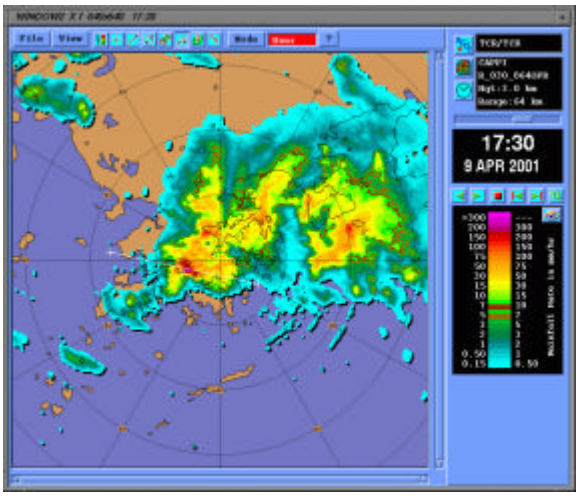

(e) 3-km CAPPI reflectivity at 5:30 p.m.

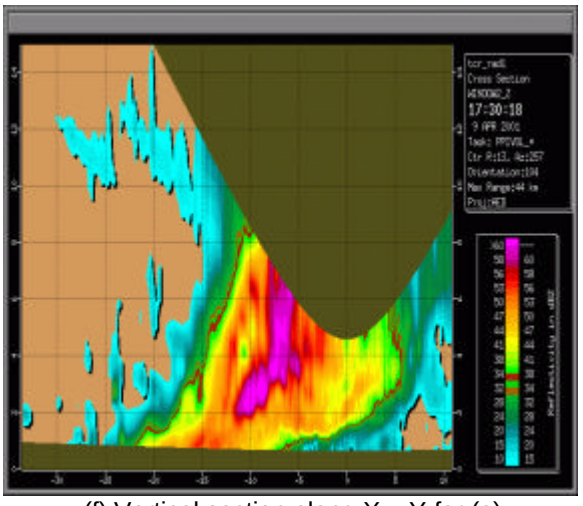

(f) Vertical section along X - Y for (e)

Fig. 5 - 3-km CAPPI reflectivity maps on the left panels (circles spaced 20 km apart). White lines X-Y are WNW-ESE segments along which corresponding vertical sections are made in the right panels (looking north, horizontal distance at 5-km interval and altitude at 2-km interval). Convergence (solid) and divergence (dashed) lines, as analyzed from AWS winds, are projected onto X-Y and marked "C" and "D" respectively. Probable vertical circulations within the hailstorm are drawn in dark arrows.

3.2 Reflectivity "back-spray"

Based on 3-km CAPPI reflectivity maps and corresponding vertical sections along selected WNW-ESE segments through the storm, the evolution of the hail-bearing convective cell in the half-hour prior to the first hail report is shown in Fig. 5. Echo intensity at the core generally exceeded 60 dBZ. The core axis tilted downwind at an angle of about 55 degrees from the vertical. The hailstorm that eventually hit downtown areas after 5:30 p.m. started off as a convective cell on the right flank of the last of three organized rainbands. While the first two rainbands were also quite intense, no hails were reported during their passage. Interestingly, hails only occurred at the stage when the first two rainbands were weakening and the hailstorm became the dominant cell in the last rainband (Fig. 5 (e)).

Focussing on the hail-bearing cell, overhanging echoes with a bounded weak echo region (BWER) were first captured at 5:06 p.m. (Fig. 5(b)). While these features were not readily identified in subsequent images, their presence at least suggested that the recycling processes for hail growth were already in progress (Wallace and Hobbs, 1977). The core of maximum reflectivity then appeared to drop momentarily downwards, nearly touching the surface at 5:18 p.m. (Fig. 5(d)). It was noted, however, that hails were not reported up to this moment in time. It could be that the storm was located over less populated areas at this point, or more likely the hail pellets, not yet quite large enough and with finite fall speed, remained suspended in the air or melted into rain on the way down.

By 5:30 p.m. when hailstones started to fall out at the surface, the vertical section seemed to depict a "fountain" of high-intensity echoes being sprayed back towards the rear of the storm (Fig. 5(f)). This could be seen as a variation or slight departure from the generalized hail trajectories proposed by Browning and Foote (1976). Looking at the vertical storm-scale circulation deduced from surface convergence and divergence, an updraft appeared to carry the hail pellets upwards, away from the core of the storm and up to a height of nearly 7 km. The hail pellets then fell into the strong rear flank downdraft, plunging through the lower troposphere before spreading out near the surface. A Doppler vertical section at the same time (Fig. 6), drawn along an E-W radial segment, corroborated the impression given by

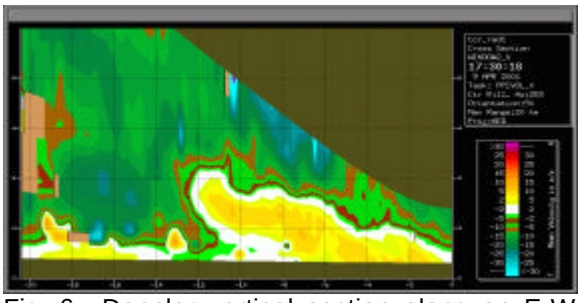

Fig. 6 - Doppler vertical section along an E-W radial segment (looking north, i.e. radar on the right; horizontal distance and altitude at 2-km interval). Maximum velocity away from radar (solid arrow) at 3-km level 10 km from radar was around 10 m s^{-1}; maximum velocity towards radar (dashed arrow) was around 30 m s^{-1} about 3 to 4 km high and 15 km from radar.

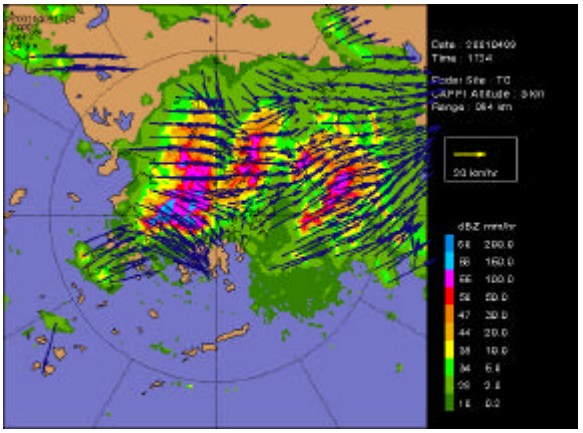

Fig. 7 - 3-km TREC vectors at 5:24 p.m. The circle marks out the 50-km range.

3.3 TREC "forward bundle"

The Observatory's nowcasting system, SWIRLS (Short-range Warning of Intense Rainstorms in Localized Systems), was also monitoring the hailstorm development. TREC (Tracking of Radar Echoes by Correlation) analysis followed the movement of individual echoes and generated a horizontal wind field at selected CAPPI level (Li *et al*., 2000). Against a general southwesterly flow of warm and humid air, winds around the hailstorm were distinctly northwesterly. A typical example of TREC vectors at 3-km height for the hailstorm case of 9 April 2001 was shown in Fig. 7. A marked feature was the tendency for the TREC vectors to be bundled together ahead of the storm, focussing towards a point of confluence where the northwesterlies were on the verge of colliding with the southwesterlies.

the reflectivity profiles.

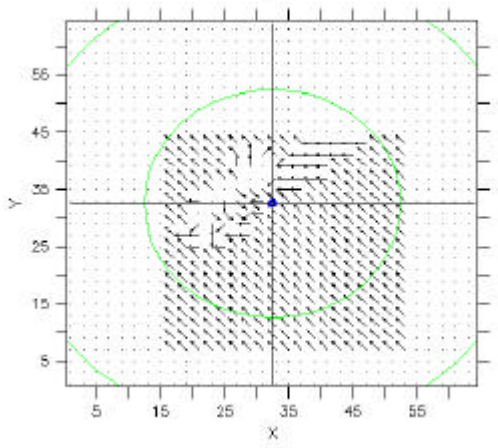

(a) Grid winds input at 1-km level

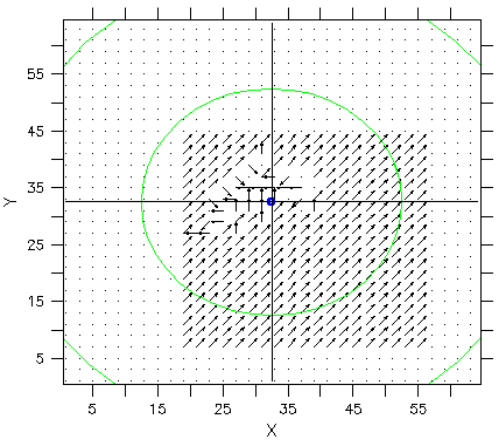

(b) Grid winds input at 3-km level

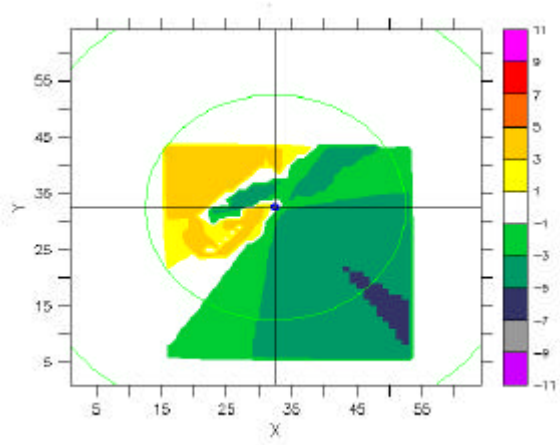

(c) 1-km level computed Doppler field

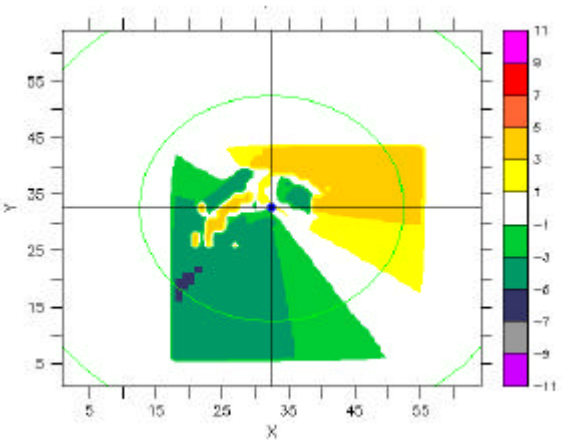

(d) 3-km level computed Doppler field

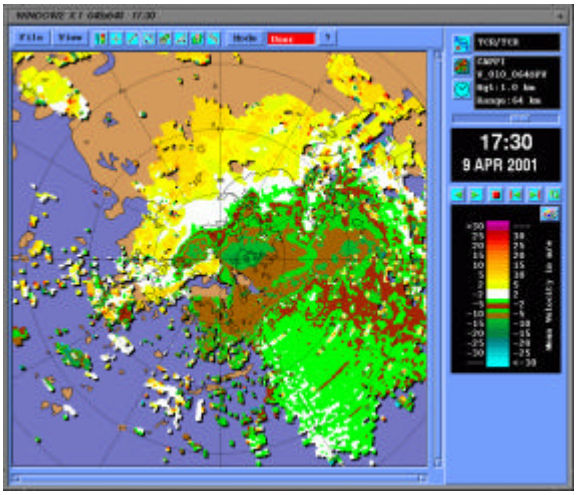

(e) 1-km level Doppler maps at 5:30 p.m.

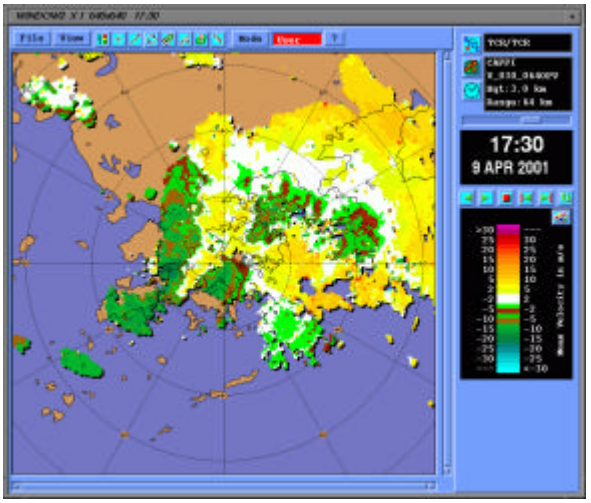

(f) 3-km level Doppler maps at 5:30 p.m.

Fig. 8 - Verification of Doppler signatures, generated from idealized conceptual storm model, at 1-km (left) and 3-km (right) levels. Top panels are the grid winds input deduced from the conceptual model (scales are arbitrary). Middle panels are the computed Doppler velocity fields (positive values away from radar; negative values towards radar), as compared with actual Doppler maps for the hailstorm case of 9 April 2001 in the bottom panels.

This bundling phenomenon remained evident in successive images, lasting for nearly half an hour when the storm cell was at its most intense in terms of maximum reflectivity. The same effect was also depicted by TREC analysis for a preceding storm a couple of hours earlier that day. That storm blew past to the north of Hong Kong and the occurrence of hails could not be verified. However, with a maximum reflectivity of over 60 dBZ at peak intensity, it was reasonable to assume that the cell was also hail-bearing. It suggested that the bundling effect is no mere coincidence, and also unlikely to be an artifact of the TREC algorithm.

One possible explanation for the bundling effect was the northwesterlies' tendency to go around the mesocyclone at the core of the cell, converging towards the front flank downdraft, sinking below and undercutting the on-rushing southwesterlies. Geometrically speaking, this corresponds to the bending of a multicell squall line into curvilinear comma shape or "hook echoes". If this hypothesis was valid, then the TREC "forward bundle" could potentially be a useful signature for hailstorm identification.

4. IDEALIZED DOPPLER PATTERNS

Velocity maps from single Doppler observation, especially for complex 3-D structure such as supercells, are not the easiest to interpret. Using the classical model as the starting framework, we attempted to construct a conceptual storm model of local relevance. In addition to observations discussed in Section 3., information from a wind profiler at Sham Shui Po, about 6 km southwest of the radar at Tate's Cairn and directly in the storm path, was also taken into consideration. Upper winds veered with height - easterly at the surface, southeasterly within the boundary layer, and southwesterly by the time they got to the 850-hPa level.

To illustrate what could be achieved, a simplistic version of the conceptual model considered just wind directions (i.e. uniform speed prescribed) in a 2-D configuration of inflow and downdraft at 1-km and 3-km levels. The resultant Doppler patterns were compared with the actual maps (Fig. 8). Despite the crudeness of the input fields, the broad Doppler features were reproduced with a fair degree of resemblance. Using increasingly sophisticated conceptual models (such as introducing vertical velocities and variation of wind speeds), we can systematically examine changes in the basic Doppler patterns in a controlled environment and then transfer the experience to a real situation.

5. NOWCASTING IMPLICATIONS

Due to differences in climate and thermodynamic conditions, hailstorms in Hong Kong were not quite the full-blown tornadic version. The hilly terrain of Hong Kong could also have disrupted the delicate balance required for optimal hail growth. Nevertheless, the dynamic processes involved remained largely similar. The observations gathered on 9 April 2001 showed that the culprit cell still went through the full repertoire of evolutionary stages in the storm spectrum. Storms were organized into multicell bands, exhibited right-propagating tendency, before the emergence of a dominant supercell eventually led to hail fallout. Typical internal features were also revealed, e.g. overhanging echoes, BWER, the airflow configuration, and relative changes in updraft/downdraft intensity as the storm matured.

For future directions, relatively unknown features such as the "reflectivity back-spray" and "TREC forward bundle" need to be documented and verified further through more observational studies as well as numerical simulations. Another major and foremost challenge is to assemble the various data types and reconcile them into one coherent picture, at a tempo that is in pace with the developing storm.

In summary, radar-based analyses, augmented by information from a mesoscale network, have the potential to identify, or even predict, the onset of severe storms on a nowcasting basis. Although the occurrence of hail ultimately depends on changes and interplay of intricate circumstances that are essentially stochastic in nature, practical guidelines and techniques for reliably identifying potential hailstorms, using the latest radar technology, are realistic and legitimate targets.

REFERENCES

Browning, K.A., and G.B. Foote, 1976: Airflow and hail growth in supercell storms and some implications for hail suppression. *Quart. J. Roy. Met. Soc.,* 102, 499-534.

Lam, C.Y., 1981: Radar observation of a tropical hailstorm. *Weather,* 36, 81-86.

Lee, B.Y., C.M. Cheng and S.C. Tai, 1996: A hailstorm in Hong Kong. *Weather*, 51, 91-94.

Li, P.W., W.K. Wong, K.Y. Chan and E.S.T. Lai, 2000: SWIRLS - An Evolving Nowcasting System. *Hong Kong Observatory Tech. Note* 100, 2-3.

Wallace, J.M., and P.V. Hobbs, 1977: *Atmospheric Science - An Introductory Survey*. Academic Press, 249.